

Bulk and homoepitaxial films of III-V nitride semiconductors: Optical studies

Jaime A. Freitas, Jr.

Naval Research Laboratory, Electronic Science and Technology Division-Electronic Materials Branch, Washington, DC 20375 USA

It is well accepted that point and extended defects play an important role on the properties of III-V nitride semiconductors. It is also essential to understand the defect formation mechanisms to obtain the necessary material control to reach the full realization of the technological potential of the wide bandgap material system. Due to the nature of the centers involved a detailed and extensive investigation must be performed in controlled samples. In this work, results obtained using a combination of defect-sensitive techniques employed to detect, identify, and verify the role of defects and impurities in the structural, optical, and electronic properties of thick freestanding GaN, bulk AlN, and homoepitaxial layers are reviewed. The sharpness and line-shapes of XRD and Raman scattering lines of AlN and GaN were employed as figures of merit to evaluate the crystalline quality and homogeneity of the bulk and epitaxial layers. Detailed luminescence studies of AlN and GaN, grown by different techniques, and homoepitaxial films show evidence of the pervasive nature of some defects.

Key words: GaN, AlN, bulk, Raman scattering, XR diffraction, photoluminescence, cathodoluminescence, homoepitaxial.

Introduction

The III-V nitride semiconductor system combines extreme values of fundamental physical and chemical properties, which promotes as one of the most promising material system for the fabrication of a variety of optical devices operating in the visible and UV spectral range, and electronic devices capable of performing at extreme conditions of power, frequency, temperature, and in harsh environments. The remarkable improvement in the quality of thin heteroepitaxial GaN and AlN films achieved in the last decade, resulting from deposition of optimized nucleation (buffer) layers and better understanding of growth processes, has allowed the fabrication and commercialization of a number of optical devices. However, the properties of these heteroepitaxial films are still seriously limiting the performance of devices demanding higher material yields, e.g., laser diodes and high-frequency/power devices. The high growth temperature usually required to produce these wide bandgap materials exacerbates fundamental material problems such as residual stress, difference in thermal expansion coefficient, low energy defect formation, and impurity incorporation. In addition, doping activation and self-compensation are difficult to control at the typically high deposition temperatures. Overcoming these limitations will require the use of native substrates to grow electronic grade homoepitaxial layers.

Typically, unintentional doped (UID) heteroepitaxial GaN films, deposited commonly on sapphire or SiC, have relatively low level of compensation and have room temperature net free-electron concentrations around 1×10^{17} electrons/cm³. These films can be doped with Mg to reproducibly achieve p-type conductivity with concentration in the lower 10^{17} holes/cm³ range [1]. The control of the conductivity type led to the fabrication and commercialization of a number of optical devices, despite the high concentration of dislocations (typically between 10^9 and 10^{10} /cm²), the limitation on the hole concentration, and the lack of identification and further reduction of the background donor concentration. A variety of models were suggested to explain the large background concentration of free-electrons observed in UID heteroepitaxial GaN films. Previous calculations have indicated that the nitrogen vacancy (N_V) could behave as the active shallow donor in GaN [2]. However, more recent first-principles calculation results have shown that the formation energy of N_V is too high to allow the incorporation of such a high concentration of donors during the growth [3]. Detailed electronic transport studies of electron irradiated samples showed conclusively that the binding energy of N_V donor is considerably higher than that observed for shallow donors in UID films [4]. Although impurities such as oxygen and silicon have been considered as the potential pervasive shallow donors in GaN, only recently detailed experimental work had identified the chemical nature of these donors [5].

Despite the considerable progress recently accomplished on the growth of bulk AlN, large area bulk AlN is not fully developed and commercialized yet. The

*Corresponding author:
Tel : +1-202-404-4536
Fax: +1-202-767-1165
E-mail: jaime.freitas@nrl.navy.mil

increasing interest on optical devices operating at deep-UV wavelength range has motivated material scientists to grow high-quality AlN heteroepitaxial layers [6-8]. AlN has been deposited by both MOCVD and MBE techniques, and more recently by hydride vapor phase epitaxy (HVPE) [9-12]. Similarly to GaN, plan view and cross-sectional TEM studies verified that the dislocation density of AlN heteroepitaxial layers are typically between $\sim 1 \times 10^8$ and $2 \times 10^{10} \text{ cm}^{-2}$ [13]. Typically, UID AlN films are insulators. Considering that AlN has the same crystallographic structure as GaN, it may be an adequate substrate option to replace sapphire and/or SiC for heteroepitaxial growth. The properties of bulk and thick freestanding (FS) III-V nitride substrates and their structural, optical, and electronic properties, and their potential application as substrates for epitaxial growth will be reviewed.

Growth of bulk and thick III-nitride substrates

Growth of crack free UID GaN films with thicknesses ranging from 100 μm to 300 μm on two-inch ($\sim 50 \text{ mm}$) c-plane sapphire substrates using the HVPE technique have been reported by a number of research groups [14-16]. The substrates are placed on a 1030 $^\circ\text{C}$ horizontal susceptor in a hot-wall HVPE reactor. Ga metal and HCl are pre-reacted to form GaCl gas, which is transported by nitrogen carrier gas to the hot growth-zone where it reacts with NH_3 and deposits GaN on the (0001) sapphire substrate. For a V/III ratio from 20 to 35, a growth rate between 30 and 100 $\mu\text{m}/\text{h}$ can be reproducibly achieved. These thick layers can be removed from the sapphire substrates by laser-assisted lift-off (248 nm line of KrF laser, with 20 ns pulse width and 50 Hz pulse rate). A laser beam energy density of 0.2 to 0.3 J/cm^2 was enough to release the nitrogen from the film forming a thin layer of liquid Ga at the film/substrate interface. To prevent fractures induced by the wafer bowing during the laser lift-off process, the GaN/sapphire templates were kept hot at a temperature below the decomposition temperature [14]. The growth surfaces of the freestanding (FS) GaN templates are extremely rough with large number of hillocks, and so they are inadequate for homoepitaxial growth. Flat, smooth surfaces are obtained after mechanical polishing, which introduces subsurface damage extending up to 4000 \AA below the surface. The polished growth surfaces (Ga-face) are reactive ion etched (RIE) to remove the damage [15]. Efficient chemical-mechanical polishing processes of the growth surface are still under development.

GaN (0002) XRD reflections obtained from the FS-UID HVPE-GaN wafers were measured at both surfaces (growth and interface) and with different wafer orientations for beam widths of 500 μm and 100 μm in order to establish the source of the rocking curve broadening. The reflection intensities versus angle of the sample

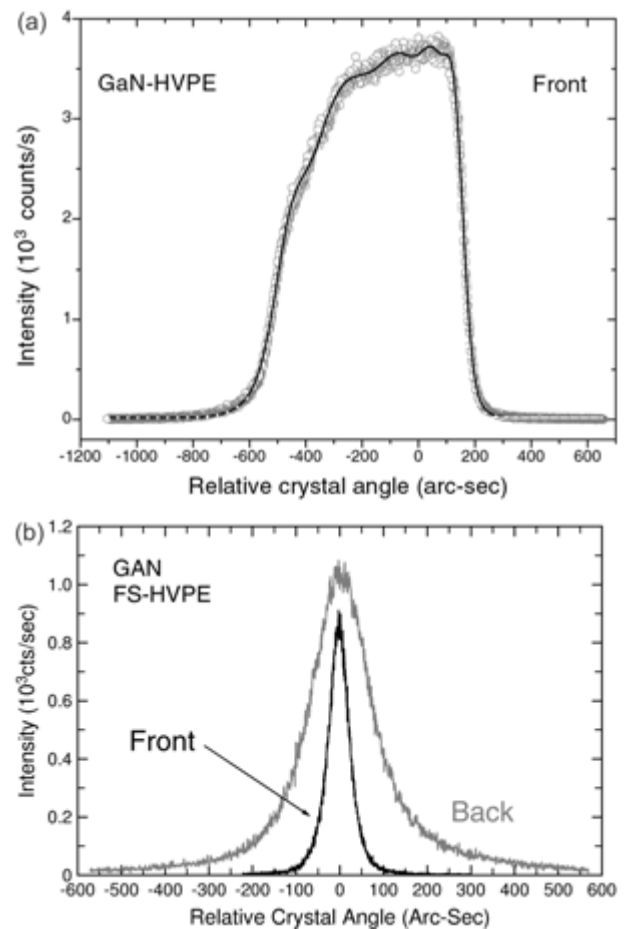


Fig. 1. X-ray rocking curves measured with 500 (a) and 100 μm (b) beam width. The spectrum in (a) is easily fitted with five Gaussian, as represented by the continuous line. Note the large difference on the FWHM between the spectrum acquired in the growth surface and the interface side of the FS-HVPE GaN substrate. After Ref. 17.

scanned with the 500 μm beam at the growth surface resulted in asymmetric lines with FWHM values between 633 and 721 arcsec, clearly showing multi-components contribution, as represented in Fig. 1a [17]. Note that these values are nearly identical, indicating that they are independent of the surface and orientation of the wafer. Measurements performed with 100 μm beam width results in sharp symmetric lines with 56 arcsec and 162 arcsec for the front and back surfaces, respectively, as shown in Fig. 1b [17]. From the difference in the horizontal scales used in the plots, we conclude that the irregular broadening observed with the larger beam is due mostly to the larger number of imperfections seen by the beam. The range of angular variations and mosaicity is effectively limited to within the region of a single grain, such that the observed broadening in this case characterizes the mosaicity within the grain. The dislocation density of these substrates is typically $\leq 10^7 \text{ cm}^{-2}$ [15].

AlN has been successfully grown by sublimation, but the high reactivity of aluminum gas at high sublimation

temperatures (typically around 2000 °C) cause problems with regards to AlN purity and crucible stability [18-20]. The largest crystal dimensions previously reported was of 470 mm³ [20, 21]. In this technique, the AlN precursor, prepared by direct reaction of aluminum powder and nitrogen at 1850 °C, was sealed in a tungsten crucible and an unseeded multi-grain crystal grew at the rate of 0.3 mm/h at 2250 °C in a nitrogen atmosphere. Samples produced by sublimation-recondensation technique are continuously improving. Boules of 15 mm diameter, grown at a 0.99 mm/h rate, are easily reproduced. These boules contain grains exceeding 1 cm, which typically show X-ray rocking curves with FWHM of around 100 arcsec or less and dislocation density less than 10⁴/cm² [22-24]. Recently, crystals with X-ray rocking curve of FWHM less than 10 arcsec and dislocation densities of 800-1000/cm² have been fabricated [25].

Spontaneously nucleated AlN crystals can be also grown from the single precursor AlCl₃·NH₃. This process requires several successive steps, namely, the synthesis of AlCl₃·NH₃, the evaporation and transport to a reaction chamber and the decomposition and growth of single crystal AlN. The dry AlCl₃·NH₃ is obtained by a sequence of few processing steps. Initially, dry AlCl₃ is produced after heating pure Al powder in dry HCl flow. The AlCl₃ is saturated with ammonia at 150 °C to form a polyammoniate polycrystalline powder with composition AlCl₃·(1.5-2.5NH₃). The polyammoniate is slowly heated in He flux at 417-420 °C to distill the white monoammoniate powder. The distilled AlCl₃·NH₃ precursor powder is placed in the cold zone of a two-zone quartz tube reactor. The temperature of the evaporator is increased up to 300-320 °C to produce AlCl₃·NH₃ vapor subsequently transported by hydrogen or helium carrier gas to the hotter zone to decompose the AlCl₃·NH₃ and grow the AlN crystals. AlN platelets with hexagonal cross-section (up to ~4 mm² and 150 μm thick) are spontaneously nucleated on graphite or quartz substrates in the temperature range between 1300°C to 1400°C. A detailed discussion of the growth technique has been reported elsewhere [26]. The AlN (0002) XRD reflections obtained from various samples fabricated from monoammoniate, using a beam width of 500 μm, show symmetric lines with full width at half maximum (FWHM) between 36 and 54 arcsec. Figure 2 shows a XRD line with FWHM of 36 arcsec measured on one hexagonal platelet with area of about 3 mm² [27]. The small FWHM value and the high intensity of the single-line indicate the high single-crystalline quality of this sample.

Large area, ranging from 0.5" to 1.75" (12 mm to 44 mm) diameter, thick (0001) AlN films have been deposited on Si and/or SiC substrates by HVPE technique, and chemically removed from the substrates [28]. These FS films were used as seeds to grow AlN boules

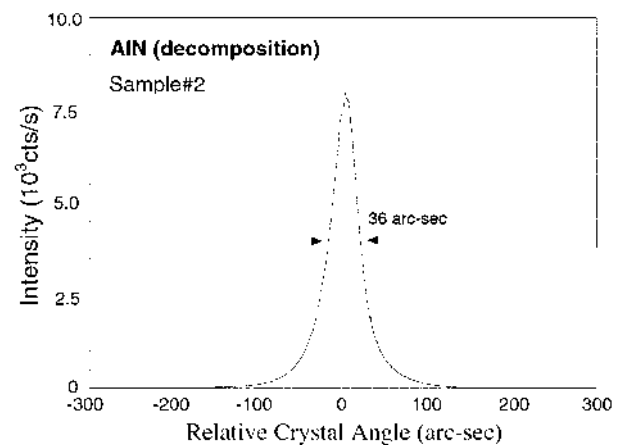


Fig. 2. XRD reflection of the c-plane AlN fabricated from monoammoniate precursor (sample#2) measured with beam width of 500 μm. After Ref. 17.

of few millimeters of thickness. Wafers of 200 μm to 500 μm of thickness were sliced from the boules. After lapping and polishing, selected wafers were used again as seeds for the growth cycle to improve the boules' crystalline quality. The typical value of the X-ray rocking curve FWHM of the (0002) reflection is of 700 arcsec, using a wide (10 mm × 1 mm) X-ray beam [29].

Structural properties of III-nitrides substrates

The hexagonal (2H) phase of GaN and AlN, a wurtzite structure belonging to the space group C_{6v}⁴ or P6₃mc, has two molecules per unit cell. Group theory predicts eight zone-center optical modes, namely 1A₁ (TO), 1A₁ (LO), 2B₁, 1E₁ (TO), 1E₁ (LO), and 2E₂. The two B₁ modes are optically inactive, but all of the six allowed modes have been observed by Raman spectroscopy [30, 31].

The first order Raman scattering (RS) spectra of a

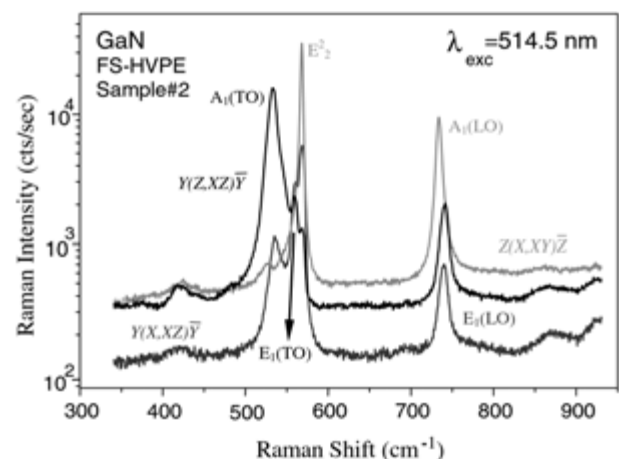


Fig. 3. Room temperature First-order polarized Raman scattering spectra of a ~167 μm thick FS-HVPE GaN substrate. After Ref. 27.

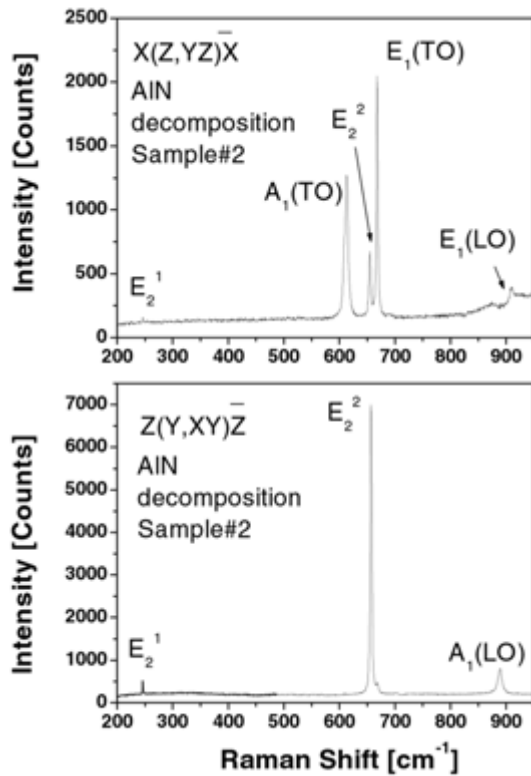


Fig. 4. Room temperature polarized Raman spectra of bulk AlN grown by thermodecomposition of $\text{AlCl}_3 \cdot \text{NH}_3$. The letters inside the brackets represent the incident and the scattered light polarization, while the letters outside of the brackets represent the direction of the incident and scattered light. After Ref. 33.

FS-HVPE GaN sample measured at room temperature for different sample orientations and light polarizations are represented in Fig. 3. Using sample orientation and polarization selection rules for the incident and scattered light we measured the first order Raman spectra with the $Z(X, XY)\bar{Z}$, $Y(Z, XZ)\bar{Y}$, and $Y(X, XZ)\bar{Y}$ symmetries, as represented in Fig. 3 by Porto's notation [32]. The Raman shift for the allowed modes $A_1(\text{TO})$, $E_1(\text{TO})$, E_2 , $A_1(\text{LO})$ and $E_1(\text{LO})$ are 534 cm^{-1} , 559 cm^{-1} , 569 cm^{-1} , 734 cm^{-1} , and 740 cm^{-1} , respectively. Analyses of the peak positions and linewidths of the observed first order phonons confirm the good crystalline quality and lower biaxial stress of the wurzite FS-HVPE GaN substrates [17].

High quality AlN crystals fabricated by thermodecomposition of aluminum chloride monoammoniate, was used to study the first order RS spectra of AlN. Figure 4. shows the Raman spectra measured at two different sample orientations and light polarizations. The Raman lines for the allowed modes $A_1(\text{TO})$, $E_1(\text{TO})$, E_2 , $A_1(\text{LO})$ and $E_1(\text{LO})$ are observed at 608.5 cm^{-1} , 667.2 cm^{-1} , 655.1 cm^{-1} , 888.9 cm^{-1} , and 909.6 cm^{-1} , respectively. The peak positions and relatively small linewidths of the phonon lines indicate that this low temperature growth process can fabricate low defect and stress free crystals. A complete discussion of the RS study will be presented elsewhere [33].

Optical and Electronic properties of III-nitride substrates

Unintentionally doped thick FS-HVPE GaN films are also typically n-type, but with much lower background free-electron concentration than HPS bulk GaN. Detailed electrical transport experiments yield a room temperature carrier mobility of $1245 \text{ cm}^2/\text{V s}$ and a carrier concentration of $6.7 \times 10^{15}/\text{cm}^3$ for an acceptor concentration of $1.7 \times 10^{15}/\text{cm}^3$ [34]. Assuming an idealistic reduction of two orders of magnitude of the background donors and acceptors, to keep the same compensation level, the maximum mobility at room temperature is expected to reach $1350 \text{ cm}^2/\text{Vs}$ [34].

Low temperature PL spectra of similar UID FS-HVPE GaN films typically show intense recombination emission lines associated with annihilation of excitons bound to neutral donors ($X\text{-D}^0$) and their phonon replicas ($n\text{LO-XD}^0$). Also commonly observed are weak zero-phonon lines from shallow-donor/shallow-acceptor pairs (DAP) recombination and their phonon replicas ($n\text{LO-DAP}$). Broad luminescence bands observed below 3.0 eV are discussed elsewhere [35]. Figure 5 shows the PL spectra of a $\sim 12 \mu\text{m}$ thick heteroepitaxial film (sample#1) from reactor 1 and a $\sim 150 \mu\text{m}$ thick FS film (sample#2) from reactor 2. The spectrum of sample#2 shows, in the 3.52 eV to 3.46 eV region, emission lines related to the excited state of the free-exciton A (FX_A^2), the ground state of the free-exciton B (FX_B^1), the ground state of the free-exciton A

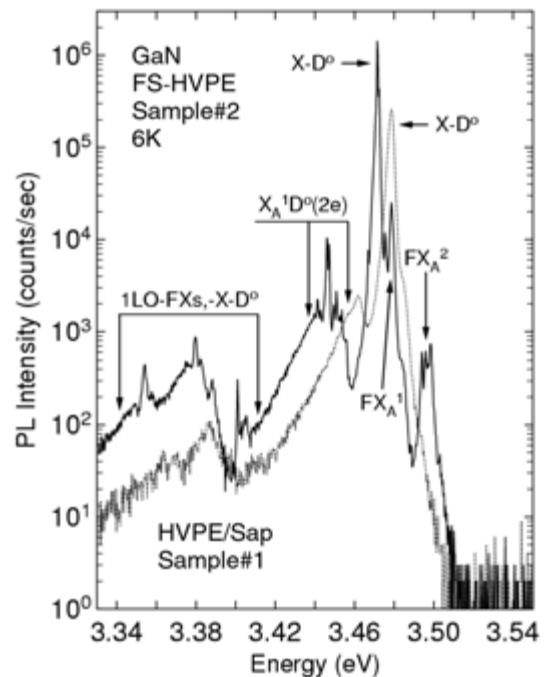


Fig. 5. 6K PL spectra of a $\sim 12 \mu\text{m}$ heteroepitaxial film (sample#1) and of a $\sim 150 \mu\text{m}$ thick freestanding film (sample#2). The presence of a variety of sharp excitonic lines in this spectral region indicates the high crystalline quality of both samples. After Ref. 36.

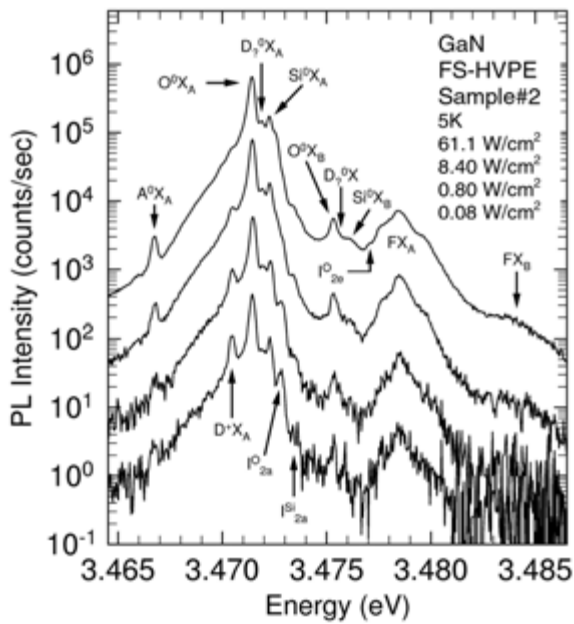


Fig. 6. High-resolution and low temperature PL spectra of the sample#2 in Fig. 3 measured with different laser power densities. The line assignments are discussed in the text. After Ref. 37.

(FX_A^1), and the dominant exciton bound to a neutral donor (XD^0). Around 3.45 eV we detect the so-called two-electron satellite (2ES) spectrum resulting from the recombination processes in which the neutral donors are left in an excited state after the exciton annihilation. Note that for energies below 3.42 eV we observe the one-phonon replicas of all features listed above. The PL spectrum of sample#1, dotted line, shows most of the features observed in the spectrum of sample#2. However, these features are broader and smeared, and shifted to higher energy due to inhomogeneous broadening and compressive strain, respectively, caused mostly by the substrate [36]. Figure 6 shows four PL spectra of sample#2 measured with higher resolution (bandpass $<100 \mu\text{eV}$) at 5K under several laser excitation intensities, as indicated in the figure. The dominant features in all spectra are emissions associated with the recombination of ground-state excitons bound to neutral donors (often designated I_2^0 , or $X-D^0$) centered around 3.4714(2) eV (all energy values are corrected for index refraction of air). The dominant peak is composed of three peaks at 3.4714(4) eV, 3.4718(9) eV, and 3.4722(8) eV (average values obtained from a number of measurements), assigned to A excitons bound to different neutral donors [37]. To identify the chemical nature of these three background donors, high-resolution IR absorption and high sensitivity SIMS measurements were carried out on the same set of samples characterized by high resolution PL spectroscopy [38]. The low temperature IR absorption spectra of sample#1 and sample#2 shows two dominant donors. The shallowest and not fully compensated donor, N1, is dominant in sample#1, while the

deepest observed donor, N2, is present at higher concentration in sample#2. A third shallow donor, N3, is observed only in sample#2. Assigning the dominant spectral lines to 1s-2p transitions, the values 30.19 ± 0.1 meV, 33.21 ± 0.1 meV, and 31.23 ± 0.1 meV are obtained for the ground state binding energies of donors N1, N2, and N3, respectively [34]. The 0.3 meV shift of the peak positions of N1 and N2 in sample#1 to higher energy as compared with sample#2 results from the biaxial strain in the heteroepitaxial sample#1. High sensitivity SIMS measurements were performed to identify the atomic nature of these donors. Special concern was dedicated to the SIMS impurity background and references for each tested impurity. C, Cl, H, O, Si, and S impurity levels were measured. The detected concentrations of O and Si are $\sim 2.4 \times 10^{16} \text{ cm}^{-3}$ and $\sim 1.2 \times 10^{17} \text{ cm}^{-3}$ for sample#1 (heteroepitaxial layer), and $\sim 2.1 \times 10^{16} \text{ cm}^{-3}$ and $\sim 3.7 \times 10^{15} \text{ cm}^{-3}$ for sample#2, respectively. The concentration of O in both samples is about the same, while sample#1 has about 34 times more Si than sample#2. The integrated absorption coefficients (IAC) for donors N1 and N2 are, respectively, 10177 and 1918 for sample#1 and 302 and 1931 for sample#2. It is important to point out that the IAC for N2 is about the same for both samples, while the N1 IAC is approximately 34 times larger for sample#1 than sample#2. These results, since none of the other investigated impurities tested by SIMS are consistent with the IR results, indicate that the shallow donors N1 and N2 observed in our HVPE samples are Si and O, respectively [38]. Assuming a similar IAC for N3 (D_7), a concentration of $2.1 \times 10^{14} \text{ cm}^{-3}$ is obtained. This extremely small value confirms the high sensitivity of FTIR spectroscopy to detect background impurities.

The three PL lines at 3.4714(4) eV, 3.4718(9) eV, and 3.4722(8) eV, represented in Fig. 6, based on the FTIR and SIMS results, are assigned to A excitons bound to O, D_7 , and Si neutral donors, respectively. This identification is consistent with the linear dependence between exciton binding energies and impurities binding energies, which follows the empirical Haynes rule with linear coefficient of 0.214 [26, 39]. In addition, the Si and oxygen impurities binding energies measured from the 2ES spectra are in excellent agreement with the IR binding energy values [40].

Although n-type bulk substrates are convenient for optical devices fabrication, semi-insulating (SI) substrates are most desirable for high-frequency devices fabrication. Material scientists have employed different approaches, adequate for each growth techniques, to reduce the background carrier concentration by controlling the growth conditions and/or doping with impurities to provide the necessary concentration of compensating centers.

Nominally undoped FS-HVPE GaN, which also are typically n-type with background carrier concentration

$\leq 1 \times 10^{17}/\text{cm}^3$, can be grown SI by using intentionally introduced transition metal impurities during the growth to compensate the residual donors. Iron concentrations lower than $1 \times 10^{17}/\text{cm}^3$ are sufficient to compensate unintentionally incorporated impurity and native defects. The resistivity of such samples measured at 250°C was $3 \times 10^5 \Omega \text{ cm}$ and at room temperature was estimated as $2 \times 10^9 \Omega \text{ cm}$ [41]. Zn doping, with concentration ranging between 10^{18} to 10^{20} cm^{-3} , was also successfully employed to grow SI GaN films with resistivity $10^{12} \Omega \text{ cm}$ at 300 K and $10^9 \Omega \text{ cm}$ at 500 K [42].

Despite the large concentration of residual oxygen in AlN grown by sublimation-recondensation, typically between $3 \times 10^{19}/\text{cm}^3$ to $1 \times 10^{21}/\text{cm}^3$, it is still SI at room temperature. This is due to the fact that most of the oxygen is not incorporated as a substitutional shallow donor, but as impurity-forming complexes with point and extended defects, which are located deep in the gap and behaving as compensating centers [43, 44]. AlN wafers grown by HVPE show a typical resistivity exceeding $10^8 \Omega \text{ cm}$ at room temperature and $10^6 \Omega \text{ cm}$ at 500 K [29].

Figure 7. shows the low temperature cathodoluminescence (CL) spectrum from 2.0 eV to approximately 6.2 eV of the a-face AlN sample 00G of Ref. 39, which has a considerable low oxygen content. In addition to an intense sharp near-band-edge (NBE) emission around 6.0 eV, two broad and featureless bands with peaks near 3.5 eV (VB) and 4.4 eV (UVB) are also observed. These bands have been previously associated with oxygen impurities [43, 44]. The high-resolution CL spectrum of the sample represented in Fig. 7 is highlighted in Fig. 8. The continuous line represents the best fit to the experimental data, represented by the open circles, using Lorentzian line shapes. The intensity and the sharpness of the lines attest to the high crystalline quality of the sample. Thermoionization

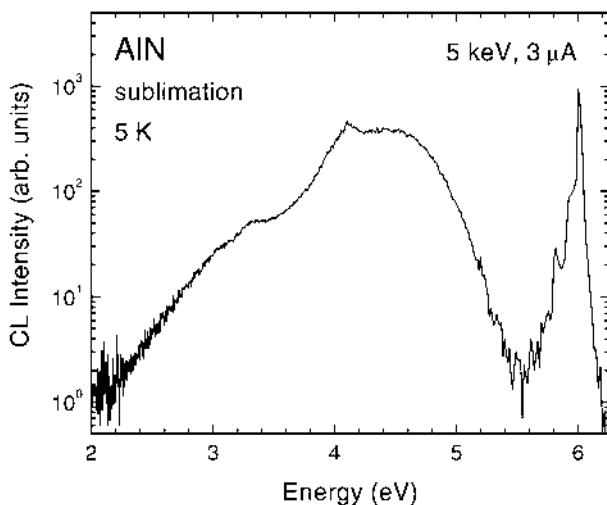


Fig. 7. 5K CL spectrum of an a-plane AlN sample fabricated by sublimation-recondensation technique. The nature of NBE and the two broad emission bands are discussed in the text. After Ref. 45.

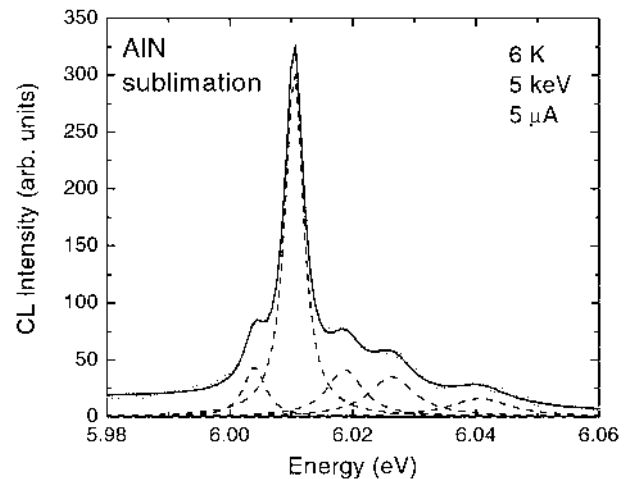


Fig. 8. High-resolution CL spectra of the sublimation AlN sample represented in Fig. 7. The assignments of the NBE lines are discussed in the text. After Ref. 45.

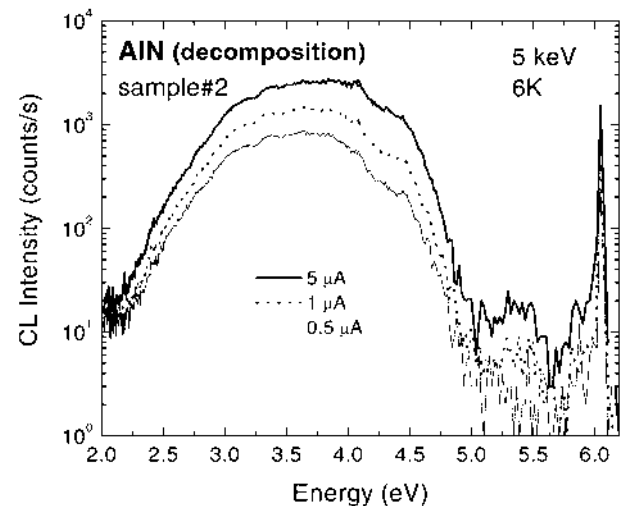


Fig. 9. Low temperature CL of a c-plane AlN (sample#2) measured at three different electron beam currents. The spectra between 2.0 eV and 4.1 eV were corrected with a calibrated light source to removed instrumental response. After Ref. 27.

studies of the recombination processes in the spectral range represented in Fig. 8 strongly suggests that the most intense line at 6.010 eV is associated with the annihilation of FX_A bound to a shallow neutral impurity with an exciton binding energy of about 15 meV [45]. The lines at 6.026 eV and 6.041 eV are observed up to 150 K, which may be related to the annihilation of free excitons [45].

Figure 9 shows the low temperature CL spectra of sample#2, grown by thermodecomposition of aluminum chloride monoammoniate, in the spectral range between 2.0 eV and 6.2 eV. The spectrum measured with a 0.5 μA e-beam current shows two broad overlapping bands with peaks at 3.6 eV and 4.3 eV. Note the similarity of all these spectral features with that observed in the CL spectrum of the sublimation sample. The spectra measured with 1.0 μA and 5.0 μA currents show an

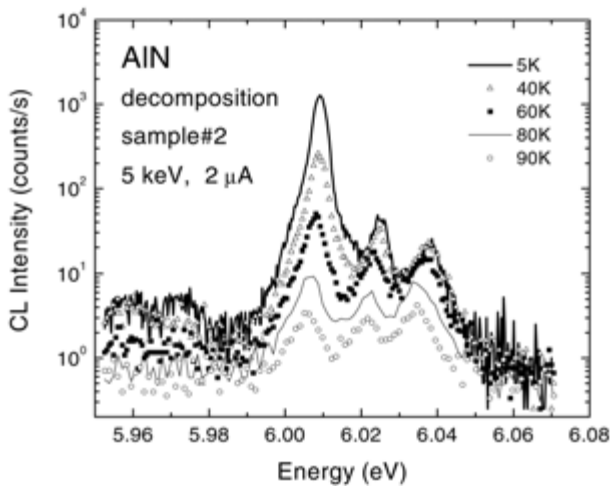


Fig. 10. High-resolution CL spectra of sample#2 measured at different temperatures. The assignments of the NBE lines are presented in the text. After Ref. 27.

additional band at 5.3 eV, whose origin is not understood [27]. Figure 10 shows the high resolution CL spectrum in the NBE spectral region measured at various temperatures of the thermodecomposition sample. The spectra show the expected systematic reduction of the CL intensity upon increasing temperature from 5K to 90K. Note that the intensity of the line at 6.0089 eV reduces at a faster rate than that of the lines at 6.0250 eV and 6.0363 eV. This behavior is commonly observed in recombination processes involving complexes, such as excitons bound to neutral impurities, where one of the components (i.e., the exciton) has lower binding energy. Based on this observation and the similarity of these spectra with that of GaN, the line at 6.0089 eV is assigned to a recombination process associated with the annihilation of exciton bound to a shallow neutral impurity (probably a donor, XD^0 , due to the small energy value), while the lines at 6.0250 eV and 6.0363 eV are assigned to recombination processes associated with the annihilation of FX. The value of the FX binding energy to the shallow donor is given by the slope, E_x/kT , of the exponential quenching curve at the highest temperatures (i.e., 17.76 meV), and it is consistent with the 16.10 meV separation between the XD^0 and FX_A lines [27]. This assignment must be verified by other techniques such as absorption or optical reflectance. The asymmetry at the lower energy side of the XD^0 line may indicate the presence of an additional line at 6.0058 meV, resolved assuming Lorentzian line shapes in the spectral fitting, which may be associated to a second shallow donor. The major difference of the lowest temperature spectrum of Fig. 10 as compared with the spectrum in Fig. 8 is the relative intensity of the three dominant bands. This observation suggests a pervasive character of the shallow donors associated with the NBE emission bands in bulk AlN. Therefore, a more systematic study

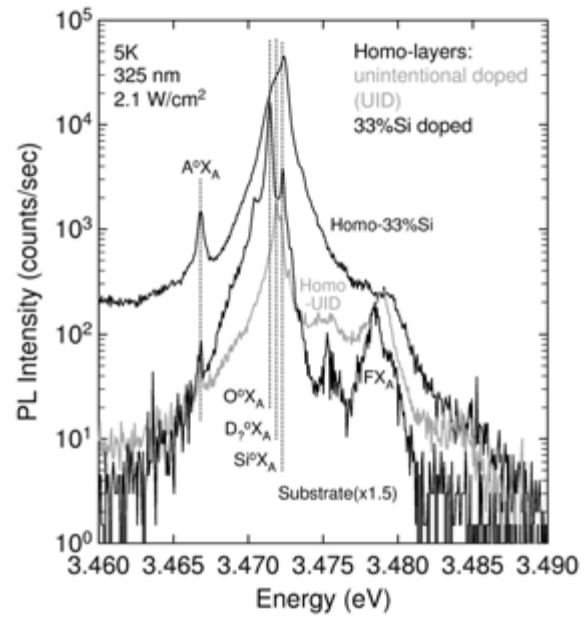


Fig. 11. High-resolution PL spectra of two MOCVD films, an UID and a Si-doped GaN, deposited on FS-HVPE substrates. The assignments of the lines associated with excitonic recombination processes are discussed in the text. After Ref. 47.

is required to access the intrinsic material properties.

CL measurements performed in samples fabricated by RF assisted vapor phase technique and HVPE show the same spectral features observed in the CL spectra of samples grown by sublimation and thermodecomposition. This observation strongly supports the idea of pervasive impurities incorporation in AlN independent of the growth technique [29, 46].

Optical and Electronic properties of homoepitaxial III-nitride films

UID and Si doped ($\leq 1 \times 10^{17}$ electron/cm³) homoepitaxial layers were deposited on FS-HVPE GaN substrates with a nominal surface roughness of about 5 nm by low pressure MOCVD. Films with thickness of about 5 μm are characterized by growth surface roughness of about 0.2 nm RMS and reduced thread dislocation density, as compared with the substrate [47]. The full-gray line spectrum of Fig. 11 marked as HOMO-UID, measured on the UID homoepitaxial film, shows a reduction of the total intensity of the neutral donor-bound exciton related emissions and a relative decrease of the intensity of the free-exciton line. The lower energy side of the neutral donor-bound exciton emission band is also reduced, suggesting that the dominant donor is that at the highest energy side of this band. This is consistent with the reduction in the concentration of the neutral donor background in the UID homoepitaxial layer. The PL spectrum of this Si-doped layer is characterized by a larger increase on the high-energy side of the neutral donor-bound excitons

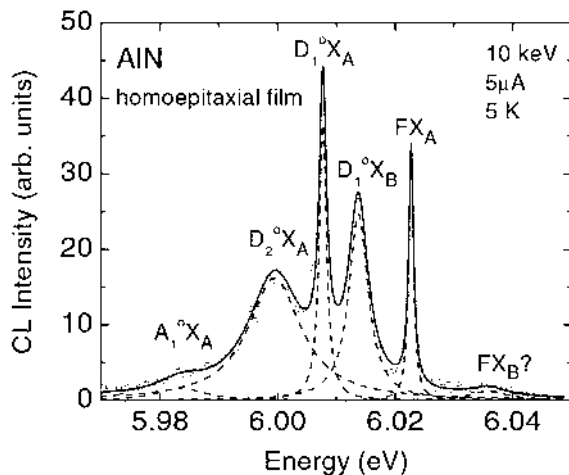


Fig. 12. High-resolution CL spectra of a MOCVD AlN film deposited on a sublimation AlN substrate. The details of the line assignments are presented in the text. After Ref. 48.

indicating that Si is in fact the shallower donor in GaN [47]. These results further strengthen the identifications of O and Si proposed in Refs. 5 and 34.

UID homoepitaxial films deposited by MOCVD on high quality AlN substrates misaligned 10° from the *c*-axis, with a nominal thickness of $0.5 \mu\text{m}$, have been investigated by variable-temperature high-resolution CL spectroscopy. The NBE CL spectrum measured at 5K, represented in Fig. 12, show six individual lines assigned to recombination processes involving the annihilation of free-excitons and excitons-bound to neutral donor and acceptor impurities. These assignments rely on detailed thermal quenching studies [48]. These lines are considerably narrower than those previously observed in the substrate, which indicates the higher structural and optical properties of the homoepitaxial layer. UID homoepitaxial HVPE films of about $2 \mu\text{m}$ thickness have also been successfully deposited on wafers grown by HVPE. The increased ratio of the intensity of NBE emission lines to the intensity of the deep emission bands of the homoepitaxial layer in comparison with the ratio of these bands in the HVPE substrates strongly suggests the improved quality of the homoepitaxial layers.

Closing remarks

Optical techniques in combination with XRD have been used to evaluate the morphological, structural, and electronic properties of bulk and homoepitaxial layers of AlN and GaN. XRD and RS results indicate that the both materials have the wurtzite crystalline structure and no detectable residual biaxial stress. Low temperature PL studies of FS HVPE-GaN and UID and Si-doped homoepitaxial layers indicates that the GaN substrates and the UID homoepitaxial films, based on the sharpness of the near bandedge emission and the number of phonon replicas, have low background level

of donors and compensating acceptors. In addition, Si and O are the dominant pervasive donors. Variable temperature CL experiment performed in bulk AlN crystals grown from aluminum monoammoniate precursor and by sublimation-recondensation processes have high crystalline quality and a residual level of pervasive impurity, which is associated with the dominant recombination processes. Similar CL studies carried out on thick freestanding AlN and homoepitaxial layer grown by HVPE show the same spectral features observed on the bulk AlN samples. These observations confirm the pervasive character of the deep defects as well as shallow impurities incorporated in AlN. A detailed study must be pursued to identify the nature of these defects.

Acknowledgement

This work was in part supported by ONR contracts N0001401WR20178 and N0001401WR20015 (Dr. C.E.C. Wood). Dr. S.K. Lee, Dr. D.D. Koleske, Dr. L.M. Ivanova, Dr. L.J. Schowalter, and Prof. G. A. Slack are gratefully acknowledged for providing the samples.

References

1. S. Nakamura, *Jpn. J. Appl. Phys.* 31 (1992) L139-142.
2. D. Jenkins, J.W. Dow, and M-H. Tsai, *J. Appl. Phys.* 72 (1992) 4130-4133.
3. C. Van de Walle, C. Stampfl, and J. Neugebauer, *J. Cryst. Growth* 189-190 (1998) 505-510.
4. D. Look, D.C. Reynolds, J.W. Hemsky, J.R. Sizelove, R.L. Jones, R.J. Molnar, *Phys. Rev. Lett.* 79 (1997) 2273-2276.
5. W.J. Moore, J.A. Freitas, Jr., G.C. B. Braga, R.J. Molnar, S.K. Lee, K.Y. Lee, I.J. Song, *Appl. Phys. Lett.* 79 (2001) 2570-2572.
6. D. Walker, X. Zhang, P. Kung, A. Saxler, S. Javadpour, J. Xu, and M. Razhegi, *Appl. Phys. Lett.* 68 (1996) 2100-2102.
7. A. Yasan, R. McClintock, K. Mayes, D. Shiell, L. Gautero, S.R. Darvish, P. Kung, and M. Razhegi, *Appl. Phys. Lett.* 83 (2003) 4701-4703.
8. K. Mayes, A. Yasan, R. McClintock, D. Shiell, S.R. Darvish, P. Kung, and M. Razhegi, *Appl. Phys. Lett.* 84 (2004) 1046-1048.
9. M. Morita, N. Ueugi, S. Isogai, K. Tsubouchi, and N. Mikoshiba, *Jpn. J. Appl. Phys.* 20 (1981) 17-23.
10. S. Yoshida, S. Mizawa, Y. Fujii, S. Takada, H. Hayada, S. Gonda, and A. Itoh, *J. Vac. Sci. Technol.* 16 (1979) 990-993.
11. Yu. Melnik, D. Tsvetkov, A. Pechnikov, I. Nikitina, N. Kuznetsov, and V. Dmitriev, *Phys. Stat. Sol. (a)* 188 (2001) 463-466.
12. J. Jasinski, Z. Liliental-Weber, Q.S. Paduano, and D.W. Weyburne, *Appl. Phys. Lett.* 83 (2003) 2811-2813.
13. Z. Liliental-Weber, H. Sohm, N. Newman, J. Washburn, *J. Vac. Sci. Technol. B* 13 (1995) 1578-1581.
14. M.K. Kelly, R.P. Vaudo, V.M. Phanse, L. Gögens, O. Ambacher, and M. Stutzmann, *Jap. J. Appl. Phys.* 38 (1999) L217-219.

15. S.S. Park, H-W. Park, S.H. Choh, *Jap. J. Appl. Phys.* 39 (1999) L1141-1142.
16. T. Paskova, V. Darakchieva, P.P. Paskov, U. Söderwall, and B. Monemar, *J. Cryst. Growth* 246 (2002) 207-214.
17. J.A. Freitas, Jr., G.C.B. Braga, W.J. Moore, J.G. Tischler, J.C. Culbertson, M. Fatemi, S.S. Park, S.K. Lee, and Y. Park, *J. Crystal Growth* 231 (2001) 322-328.
18. G.A. Cox, D.O. Cummins, K. Kawabe, and R.H. Tredgold, *J. Phys. Chem. Sol.* 28 (1967) 543-548.
19. T. Ishii, T. Sato, and M. Iwata, *Mineral. J.* 6 (1971) 323, *Denki Kagaku* 38 (1970) 429-432.
20. G.A. Slack and T.F. MacNelly, *J. Cryst. Growth* 34 (1976) 263-279.
21. G.A. Slack and T.F. MacNelly, *J. Cryst. Growth* 42 (1977) 560-563.
22. L.J. Schwalter, Y. Susterman, R. Wang, I. Bhat, G. Arunmozhi, and G.A. Slack, *Appl. Phys. Lett.* 76 (2000) 985-987.
23. L.J. Schwalter, J.C. Rojo, G.A. Slack, Y. Susterman, R. Wang, I. Bhat, and G. Arunmozhi, *J. Cryst. Growth* 211 (2000) 78-81.
24. J.C. Rojo, G.A. Slack, K. Morgan, B. Raghathamachar, M. Dudley, and L.J. Schwalter, *J. Cryst. Growth* 231 (2000) 317-321.
25. B. Raghathamachar, M. Dudley, J.C. Rojo, K. Morgan, and L.J. Schowalter, *J. Cryst. Growth* 250 (2003) 244-250.
26. A.A. Pletyushkin and N.G. Slavina, *Izvestiya Akademii Nauk SSSR, Neorg. Mater.* 4 (1968) 893-896.
27. J.A. Freitas, Jr., G.C.B. Braga, E. Silveira, J.G. Tischler, and M. Fatemi, *Appl. Phys. Lett.* 83 (2003) 2564-2566.
28. A. Nikolaev, I. Nikina, A. Zubrilov, M. Mynbaeva, Yu. Melnik, and V. Dmitriev, *MRS Internet J. Nitride Semicond.* 595 (2000) W6.5.1-3.
29. Yu. Melnik, V. Soukhoveev, V. Ivantsov, V. Sizov, A. Pechnikov, K. Tsvetkov, O. Kovalenkov, V. Dmitriev, A. Nikolaev, N. Kuznetsov, E. Silveira, and J.A. Freitas, Jr., *Phys. St. Sol. (a)* 200 (2003) 22-25.
30. J.A. Freitas, Jr. and M.A. Khan, *Mat. Res. Soc.* 339 (1994) 547-552.
31. L. Bergman, M. Dutta, and R.J. Nemanich, in *Raman Scattering in Materials Science*, ed. W.H. Weber and R. Merlin, Springer Series in Materials Science 42 (2000) 2730-313.
32. S.P.S. Porto, in *light Scattering Spectra of Solids*, ed. G.B. Wright (New York 1969) p.1-24.
33. J. Tischler and J.A. Freitas, Jr., *Appl. Phys. Lett.* 85 (2004) 1943-1945.
34. D.C. Look and J.R. Sizelove, *Appl. Phys. Lett.* 79 (2001) 1133-1135.
35. J.A. Freitas, Jr., O.H. Nam, R.F. Davis, G.V. Saparin, S.K. Obyden, *Appl. Phys. Lett.* 72 (1998) 2990-2992.
36. J.A. Freitas, Jr., G.C.B. Braga, W.J. Moore, S.K. Lee, K.Y. Lee, I.J. Song, R.J. Molnar, P. Van Lierde, *Phys. Stat. Sol. (a)* 188 (2001) 457-461.
37. J.A. Freitas, Jr., W.J. Moore, B.V. Shanabrook, G.C. B. Braga, S.K. Lee, S.S. Park, J.Y. Han, *Phys. Rev. B* 66 (2002) 233311/1-4.
38. W.J. Moore, J.A. Freitas, Jr., G.C. B. Braga, R.J. Molnar, S.K. Lee, K.Y. Lee, I.J. Song, *Appl. Phys. Lett.* 79 (2001) 2570-2572.
39. J.R. Haynes, *Phys. Rev. Lett.* 4 (1960) 361-363.
40. W.J. Moore, J.A. Freitas, Jr., S.K. Lee, S.S. Park, J.Y. Han, *Phys. Rev. B* 65 (2002) 81201/1-4.
41. R.P. Vaudo, X. Xu, A. Salant, J. Malcarne, and G. Brandes, *Phys. Stat. Sol. (a)* 200 (2003) 18-21.
42. N.I. Kuznetsov, A.E. Nikolaev, A.S. Zubrilov, Yu.V. Melnik, V.A. Dmitriev, *Appl. Phys. Lett.* 75 (1999) 3138-40.
43. G. A. Slack, L. J. Schowalter, D. Morelli, J. A. Freitas Jr., *J. Crystal Growth* 246 (2002) 287-298.
44. R.A. Youngman and J.H. Harris, *J. Am. Ceram. Soc.* 73 (1990) 3238-3246.
45. E. Silveira, J.A. Freitas, Jr., G.A. Slack, and L.J. Schowalter, *Phys. Stat. Sol. (c)* 0 (2003) 2618-2622.
46. V. Noveski, R. Schlessler, J.A. Freitas, Jr., S. Mahajan, S. Beaudoin, and Z. Sitar, *Mat. Res. Soc. Proc.* 798 (2003) Y 2.8.1-6.
47. J.A. Freitas, Jr., W.J. Moore, B.V. Shanabrook, G.C. B. Braga, S.K. Lee, S.S. Park, J.Y. Han, and D.D. Koleske, *J. Crystal Growth* 246 (2002) 307-314.
48. E. Silveira, J.A. Freitas, Jr., Kneissl, M., Treat, D.W. Johnson, N.M., G.A. Slack, and L.J. Schowalter, *Appl. Phys. Lett.* 84 (2004) 3501-3503.